Chemical Science

ROYAL SOCIETY OF CHEMISTRY

EDGE ARTICLE

View Article Online
View Journal | View Issue



Cite this: *Chem. Sci.*, 2025, **16**, 16744

All publication charges for this article have been paid for by the Royal Society of Chemistry

Received 18th June 2025
Accepted 7th August 2025

DOI: 10.1039/d5sc04487a

rsc.li/chemical-science

# A malondialdehyde-activated fluorescent probe reveals lysosomal dysfunction in atherosclerosis

Xia Zhang,†[a] Guocheng Li,†[a] Yanhua Li,*[a] Na Li,*[a] Wei Pan*[a] and Bo Tang[ab]

Lysosomes, serving as the digestive centers in cells, play a crucial role in lipid metabolism, inflammatory regulation, and cellular homeostasis. The bidirectional vicious cycle between lysosomal dysfunction and oxidative stress synergistically promotes the occurrence, development and instability of atherosclerosis. Therefore, accurate assessment of lysosomal oxidative stress contributes to monitoring atherosclerosis progression and facilitating early diagnosis. Herein, we constructed a malondialdehyde-activated fluorescent probe (Lyso-Np-Hy) by combining naphthalimide dye with a hydrazine group to evaluate lysosomal oxidative stress in atherosclerosis. Lyso-Np-Hy possessed high specificity and sensitivity to malondialdehyde in living cells and showed excellent subcellular localization of lysosomes. Importantly, the probe could monitor the malondialdehyde levels in lysosomes at different stages of atherosclerosis. This study provides a novel chemical tool for evaluating lysosomal dysfunction and tracking the progression of atherosclerosis.

## Introduction

Atherosclerosis is a chronic disease induced by inflammatory cell infiltration and lipid deposition.[1–4] Lysosomes, as crucial cellular digestive organelles, contain numerous hydrolases that play important regulatory roles in maintaining intracellular lipid homeostasis.[5–8] Moreover, lysosomes protect vascular tissues from oxidative stress and inflammation by degrading damaged organelles and pathogens.[9,10] However, lysosomal dysfunction can promote lipid accumulation and inflammatory response, directly contributing to the formation and instability of atherosclerotic plaques.[11,12] Lysosome dysfunction has been identified as one of the key mechanisms of the pathogenesis of atherosclerosis.[13–15] Redox imbalance in the cell can lead to abnormal diffusion of reactive oxygen species (ROS) in lysosomes, resulting in membrane rupture and subsequent dysfunction.[16–18] In turn, lysosomal dysfunction inhibits the autophagic flux, further promoting the production of ROS. Lysosomal dysfunction and oxidative stress mutually reinforce by a positive feedback mechanism, synergistically driving the progression of atherosclerosis. Hence, assessing oxidative stress in lysosomes is important for early diagnosis and risk classification of atherosclerosis.

Unsaturated lipids are the most affected biomacromolecules by oxidative stress.[19,20] As the end product of lipid peroxidation, malondialdehyde (MDA) has been considered an important biomarker for the assessment of oxidative stress.[21–23] MDA can contribute to lysosomal dysfunction by disrupting the lysosomal membrane permeability and increasing the lysosomal pH, thereby accelerating the development of atherosclerosis.[24–26] Compared with ROS, MDA possesses higher stability, making it more suitable as a biomarker for oxidative stress. Accurate tracking of MDA levels in lysosomes is critical for assessing oxidative stress-induced lysosomal dysregulation and atherosclerosis progression. The thiobarbituric acid (TBA) kit is traditionally used for MDA detection, with which it is difficult to accurately monitor MDA in living cells and *in vivo* due to complex operation and poor specificity.[27,28] Fluorescence technology with non-invasive imaging, high sensitivity and specificity provides an attractive tool for imaging MDA *in vivo*.[29–33] Constructing a fluorescent probe that can precisely locate lysosomes in plaque and visualize MDA fluctuations would be of great significance for evaluating atherosclerosis development and plaque stability.

In this study, we developed a lysosome-targeted fluorescent probe to assess lysosomal oxidative stress in atherosclerotic plaques. The probe (Lyso-Np-Hy) consisted of a fluorophore (naphthalimide), a targeting group (morpholine), and a recognition moiety (hydrazine) (Scheme 1). The reaction of MDA with hydrazine inhibits photo-induced electron transfer (PET) from hydrazine to naphthalimide, thus inducing strong fluorescence emission. Lyso-Np-Hy could specifically detect the significant increase of MDA levels in lysosomes during cellular oxidative stress and foam cell formation. Furthermore, *in vivo* imaging

[a]*College of Chemistry, Chemical Engineering and Materials Science, Key Laboratory of Molecular and Nano Probes, Ministry of Education, Collaborative Innovation Center of Functionalized Probes for Chemical Imaging in Universities of Shandong, Institute of Molecular and Nano Science, Shandong Normal University, Jinan 250014, P. R. China. E-mail: liyanhua@sdnu.edu.cn; lina@sdnu.edu.cn; panwei@sdnu.edu.cn*

[b]*Laoshan Laboratory, Qingdao 266237, P. R. China*

† These authors contributed equally.

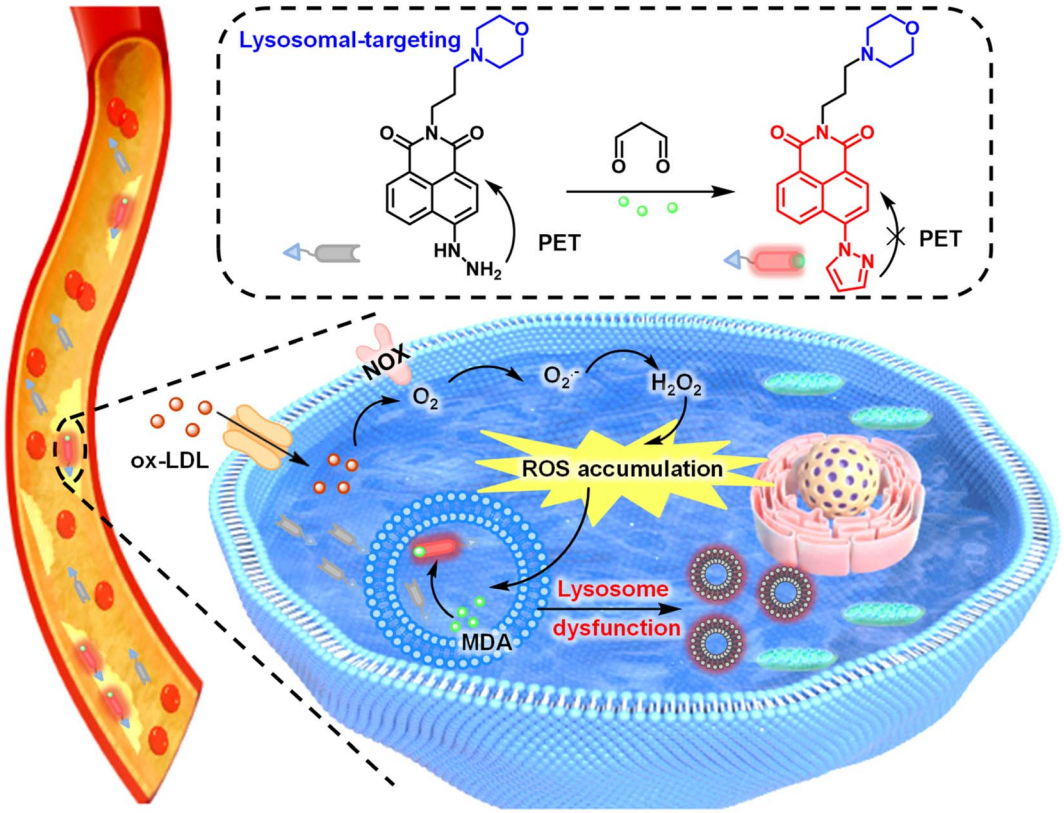


Scheme 1 Schematic diagrams of the molecular structure, response mechanism and lysosomal MDA imaging of Lyso-Np-Hy.

revealed that lysosomal MDA levels elevated obviously when no significant plaque appeared after the mice were fed with a high-fat diet for 8 weeks, suggesting that MDA may serve as an early marker of atherosclerosis. The fluorescent probe presents a promising strategy for *in vivo* assessment of lysosomal dysfunction and holds potential for facilitating early diagnosis of atherosclerosis.

## Results and discussion

### Synthesis and characterization of Lyso-Np-Hy

Due to its excellent photostability and structural tunability, naphthalimide was selected as a fluorophore for imaging MDA. Lysosome-targeting morpholine was modified on naphthalimide with an amide bond, and then hydrazine was conjugated by a nucleophilic substitution reaction to obtain Lyso-Np-Hy. The synthesis procedure and structure characterization of Lyso-Np-Hy are shown in Scheme S1 and Fig. S1–S4. The PET from the hydrazine group to the naphthalimide resulted in fluorescence quenching. When reacting with MDA, the PET process was inhibited, and the fluorescence of the probe was restored. The products before and after the probe reaction with MDA were further characterized by HRMS. After MDA incubation, a reactant of the probe and MDA was observed (Fig. 1A and B), indicating that the probe could react with MDA to restore its fluorescence. Next, the optical properties of Lyso-Np-Hy were evaluated. As shown in Fig. 1C, the characteristic absorption peak of Lyso-Np-Hy was at about 445 nm, while the absorption peak blue shifted to 355 nm with addition of MDA. Moreover, the absorption peak at 355 nm gradually enhanced with an increase in the MDA concentration from 0 to 10 μM (Fig. S5). The fluorescence response of Lyso-Np-Hy to MDA was investigated, and the fluorescence emission of the probe at 470 nm was significantly enhanced after the addition of MDA (Fig. 1D). With the increase of MDA, the probe exhibited a significantly enhanced fluorescence signal at 470 nm and a good linear relationship between fluorescence intensity and the MDA concentration ($F = 65$ [MDA] $-2.72$ and $R^2 = 0.9937$) (Fig. 1E and F). And the limit of detection (LOD) was calculated to be 169 nM at 3 S $k^{-1}$. Next, an inhibition experiment was carried out to verify the specificity of the probe's response to MDA. After MDA was co-incubated with the MDA inhibitor (2-HOBA), the fluorescence intensity of the probe significantly decreased (Fig. S6), suggesting that the fluorescence enhancement of the probe was caused by MDA. The kinetic curves showed that the reaction between the probe and MDA was completed within 1 h (Fig. 1G).

To evaluate the specificity of Lyso-Np-Hy for MDA, we selected a variety of active substances, including metal ions, amino acids, reducing agents and oxidants to treat the probe. As expected, only the fluorescence intensity of the probes remarkably increased after incubation with MDA. In contrast, the fluorescence intensity remained largely unchanged with other active substances (Fig. 1H). As lysosomes are acidic organelles, we further evaluated the responsive behavior of the

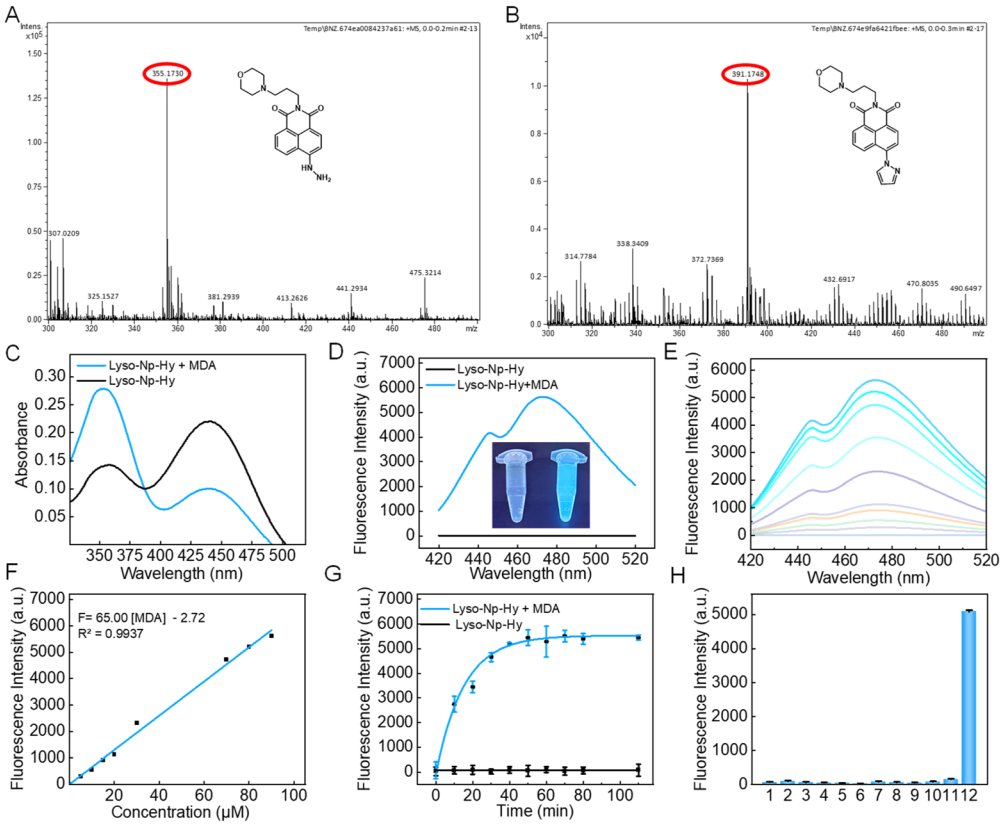


Fig. 1 The HRMS spectrum of Lyso-Np-Hy before (A) and after (B) treatment with MDA. (C) The UV absorption spectrum of Lyso-Np-Hy before and after addition of MDA. (D) The fluorescence intensity of Lyso-Np-Hy before and after addition of MDA. (E) The fluorescence intensity of Lyso-Np-Hy with different concentrations of MDA. (F) Linear relationship between the fluorescence intensity at 470 nm with the MDA concentration. (G) The fluorescence intensity of Lyso-Np-Hy at different times after incubation with MDA. (H) The interference testing of Lyso-Np-Hy. 1 control, 2 $Na^+$, 3 $Mg^{2+}$, 4 $K^+$, 5 glucose, 6 TCEP, 7 GSH, 8 L-cysteine, 9 L-arginine, 10 $H_2O_2$, 11 ATP, and 12 MDA.

probe under different pH conditions. As shown in Fig. S7, the probe exhibited the strongest response to MDA at pH 5.5, suggesting that this probe was applied for detecting MDA within acidic lysosomes. Moreover, the fluorescence intensity of Lyso-Np-Hy remained stable for 7 days, and the fluorescence intensity of the probe after reacting with MDA remained basically unchanged for 7 days (Fig. S8), demonstrating excellent photostability. These above results indicated that Lyso-Np-Hy possessed high sensitivity, specificity and photostability, which was suitable for imaging lysosomal MDA in complex living systems.

### Fluorescence imaging of intracellular MDA in living cells

Inspired by the *in vitro* detection data, Lyso-Np-Hy was used to image endogenous MDA in living cells to assess oxidative stress. First, we investigated the cytotoxicity of Lyso-Np-Hy by MTT assay.[34,35] The toxicity of the probe to macrophages (RAW 264.7 cells) was negligible, indicating that the probe had good biocompatibility (Fig. S9). The RAW 264.7 cells were incubated with $H_2O_2$ to induce the production of MDA. Then, the cells were treated with Lyso-Np-Hy for 2 h and analyzed by confocal laser scanning microscopy (CLSM). As shown in Fig. 2A, with an increase in the $H_2O_2$ concentration, the intracellular green fluorescence signal was significantly enhanced, suggesting an increase in MDA expression under oxidative stress. However, the green fluorescence decreased after the cells were treated with 2-HOBA (MDA inhibitor) (Fig. 2A and B), which further confirmed that Lyso-Np-Hy could reflect the fluctuations of MDA in the living cells. The formation of foam cells is one of the major factors of atherosclerosis. Using the probes, we further revealed the level of MDA in the foam cells. The transformation of macrophages into foam cells was induced by ox-LDL, and the levels of ROS in the cells were first assessed. As shown in Fig. S10 and S11, the levels of $H_2O_2$ and ROS significantly increased after incubation with ox-LDL, indicating that the formation of foam cells might lead to intracellular oxidative stress to promote the increase in MDA. As expected, the cells showed the remarkable enhancement of green fluorescence, suggesting an increase in MDA after ox-LDL stimulation (Fig. 2C). Furthermore, to further verify the fluorescence response of the probe to MDA in foam cells, the cells were pretreated with 2-HOBA. As shown in Fig. 2D, the green fluorescence of the 2-HOBA pretreated cells decreased by about 1.96-fold compared with untreated foam cells, which was due to the reduction of MDA by 2-HOBA. These results indicated that the probe possessed excellent specificity for MDA in living cells.

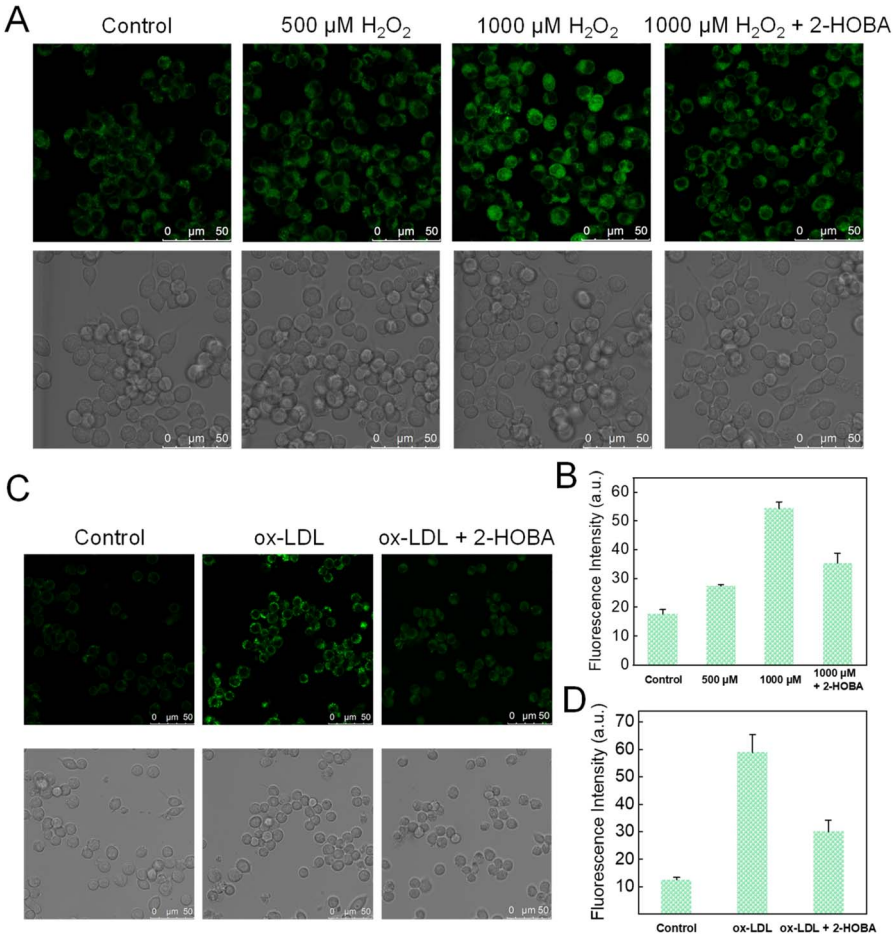


Fig. 2 (A) Fluorescence imaging of endogenous MDA under oxidative stress by CLSM. (B) The corresponding fluorescence quantization of (A). (C) Fluorescence imaging of MDA in foam cells. (D) The corresponding fluorescence quantization of (C).

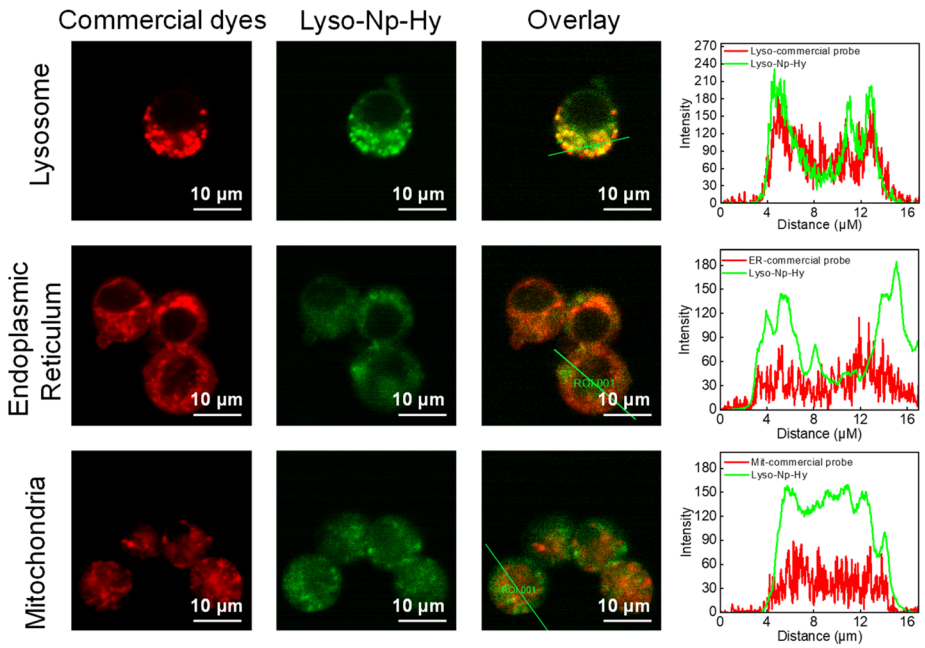


Fig. 3 Co-localization images of Lyso-Np-Hy with organelles in foam cells, and the corresponding overlapping curves of Lyso-Np-Hy with organelle dyes. The green channel: Lyso-Np-Hy ($\lambda_{ex}$ = 405 nm and $\lambda_{em}$ = 420–480 nm); the red channel: FluoLyso-Deep Red ($\lambda_{ex}$ = 633 nm and λem = 650–750 nm), ER-Tracker Green ($\lambda_{ex}$ = 488 nm and $\lambda_{em}$ = 500–600 nm) and Mito-Tracker Green ($\lambda_{ex}$ = 488 nm and $\lambda_{em}$ = 500–600 nm).

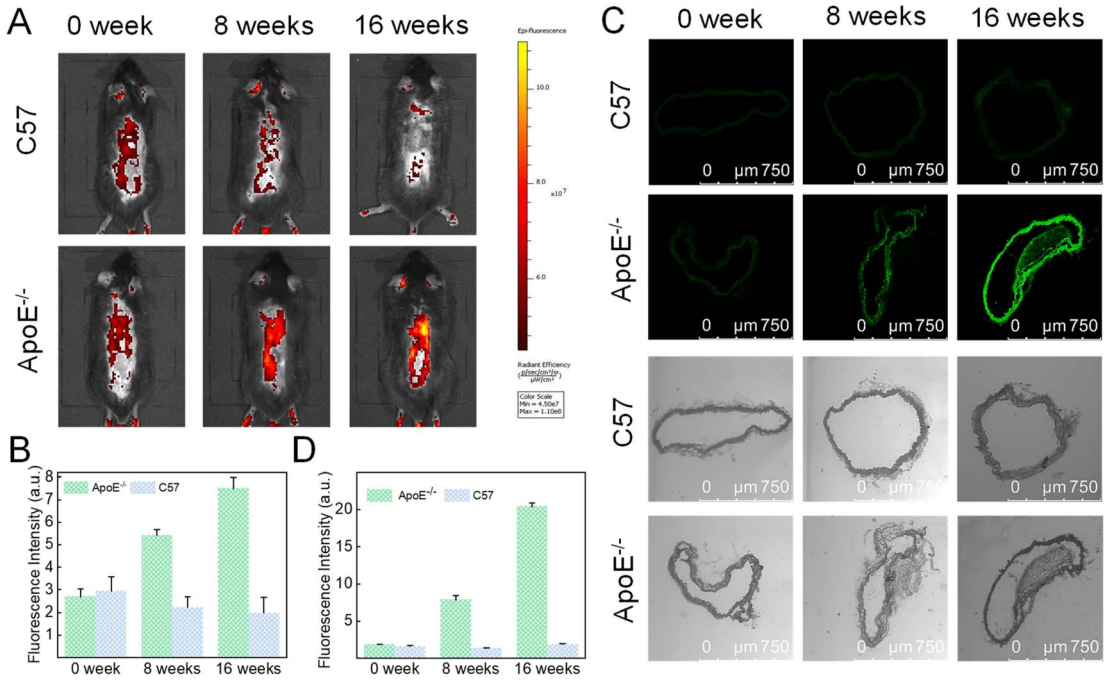


Fig. 4 (A) Fluorescence imaging of ApoE$^{-/-}$ mice and C57 mice at different periods after injection of Lyso-Np-Hy by IVIS. (B) The corresponding fluorescence intensity quantization of (A). (C) Frozen section of ApoE$^{-/-}$ mice and C57 mice at different periods by CLSM. (D) The corresponding fluorescence intensity quantization of (C).

Next, we investigated the subcellular distribution of the probes in foam cells by co-localization assay. The RAW 264.7 cells were first incubated with ox-LDL for 24 h and then with Lyso-Np-Hy and organelle dyes (FluoLyso-Deep Red, ER-Tracker Green and Mito-Tracker Green). As shown in Fig. 3, the green fluorescence of the probes and the red fluorescence of FluoLyso-Deep Red showed a good correlation with a high Pearson's colocalization coefficient of 0.83. For comparison, the fluorescence overlaps between the probes and mitochondria and endoplasmic reticulum were poor, and Pearson colocalization coefficients were 0.66 and 0.62, respectively. These results indicated that the probes could specifically locate in the lysosome.

### Specific imaging of atherosclerotic plaque *in vivo*

Since the probe has a good fluorescence response to MDA in living cells, we further explored whether the probe could be employed to selectively visualize the atherosclerotic plaque *in vivo*. The atherosclerosis model was established by feeding apolipoprotein E-deficient (ApoE$^{-/-}$) mice with a high-fat diet and C57 mice with a normal diet as the control group. Oil red O staining showed obvious atherosclerotic plaques in the vascular lumen of ApoE$^{-/-}$ mice after 16 weeks of feeding, suggesting the successful construction of the atherosclerosis model (Fig. S12). Subsequently, the fluorescence imaging of atherosclerotic plaques using Lyso-Np-Hy was studied in ApoE$^{-/-}$ mice. As shown in Fig. 4A, the fluorescence in ApoE$^{-/-}$ mice was significantly enhanced compared with normal mice after 16 weeks of high-fat feeding. In addition, the fluorescence intensity in ApoE$^{-/-}$ mice was gradually enhanced with the development of atherosclerosis (Fig. 4B). Next, the aortas and major organs (heart, liver, spleen, lung, and kidney) were dissected and imaged by IVIS (Fig. S13 and S14). The imaging results were consistent with the above results. To further verify the ability of Lyso-Np-Hy to image plaques, the aortas were frozen and sectioned and confocal imaging of the aortas was performed. Fig. 4C showed the enhancement in the Lyso-Np-Hy fluorescence signal in the aorta with the plaque development. And the fluorescence intensity increased 4.18-fold and 10.8-fold, respectively, at 8 and 16 weeks of feeding (Fig. 4D). These results suggested that Lyso-Np-Hy had great potential in monitoring atherosclerosis.

## Conclusion

In summary, we developed an oxidative stress detector (Lyso-Np-Hy) for imaging endogenous MDA in atherosclerotic plaques to assess lysosomal dysfunction and disease progression. This probe exhibited high sensitivity, high specificity and good compatibility, enabling the detection of MDA in lysozymes of living cells under oxidative stress. Using the probe, we observed that lysosomal MDA increased significantly in foam cells and atherosclerotic plaques. Considering the strong association between atherosclerosis and MDA accumulation, we speculate that MDA may serve as a potential biomarker for atherosclerosis. This study provides new insights into the pathogenesis of atherosclerosis and other oxidative stress-related diseases.

## Ethical statement

Animal experiments were reviewed and approved by the Ethics Committee of Shandong Normal University, Jinan, P. R. China

(approval number AEECSDNU2024102). All the animal experiments complied with relevant guidelines of the Chinese government and regulations for the care and use of experimental animals.

## Author contributions

X. Zhang and G. Li carried out all the experiments. Y. Li, N. Li, W. Pan and B. Tang guided the process. X. Zhang, G. Li, Y. Li, N. Li and W. Pan co-wrote the manuscript.

## Conflicts of interest

There are no conflicts to declare.

## Data availability

A detailed materials list, experimental procedures and supporting data have been provided in the SI. Further data will be made available on request. See DOI: **https://doi.org/10.1039/d5sc04487a**.

## Acknowledgements

This work was supported by the National Natural Science Foundation of China (22274089, 22206117, and 22374092) and the Project of Shandong Provincial Center for Fundamental Science Research (YDZX2024150). The schematic diagram (Scheme 1) was drawn using Figdraw.

## Notes and references

1 Y. Döring, E. P. C. van der Vorst and C. Weber, *Nat. Rev. Cardiol.*, 2024, **21**, 824–840.
2 R. A. Rosalia, M. Klincheva, M. Klimkarov, R. Zimoski, N. Hristov, P. Milojevik and Z. K. Mitrev, *Eur. Heart J.*, 2020, **41**, ehaa946.3151.
3 A. Heyde, D. Rohde, C. S. McAlpine, S. Zhang, F. F. Hoyer, J. M. Gerold, D. Cheek, Y. Iwamoto, M. J. Schloss, K. Vandoorne, O. Iborra-Egea, C. Muñoz-Guijosa, A. Bayes-Genis, J. G. Reiter, M. Craig, F. K. Swirski, M. Nahrendorf, M. A. Nowak and K. Naxerova, *Cell*, 2021, **184**, 1348–1361.
4 S. Zaman, J. H. Wasfy, V. Kapil, B. Ziaeian, W. A. Parsonage, S. Sriswasdi, T. J. A. Chico, D. Capodanno, R. Colleran, N. R. Sutton, L. Song, N. Karam, R. Sofat, C. Fraccaro, D. Chamié, M. Alasnag, T. Warisawa, N. Gonzalo, W. Jomaa, S. R. Mehta, E. E. S. Cook, J. Sundström, S. J. Nicholls, L. J. Shaw, M. R. Patel and R. K. Al-Lamee, *Lancet*, 2025, **405**, 1264–1312.
5 H. Zhu, Q. Li, T. Liao, X. Yin, Q. Chen, Z. Wang, M. Dai, L. Yi, S. Ge, C. Miao, W. Zeng, L. Qu, Z. Ju, G. Huang, C. Cang and W. Xiong, *Nat. Methods*, 2021, **18**, 788–798.
6 L. K. K. Holland, I. Ø. Nielsen, K. Maeda and M. Jäättelä, *Cell*, 2020, **181**, 748.
7 M. Savini, A. Folick, Y.-T. Lee, F. Jin, A. Cuevas, M. C. Tillman, J. D. Duffy, Q. Zhao, I. A. Neve, P.-W. Hu, Y. Yu, Q. Zhang, Y. Ye, W. B. Mair, J. Wang, L. Han, E. A. Ortlund and M. C. Wang, *Nat. Cell Biol.*, 2022, **24**, 906–916.
8 S. Singh, U. E. Dransfeld, Y. A. Ambaw, J. Lopez-Scarim, R. V. Farese and T. C. Walther, *Cell*, 2024, **187**, 6820–6834.
9 C. Li, Z. Zhao, Y. Luo, T. Ning, P. Liu, Q. Chen, Y. Chu, Q. Guo, Y. Zhang, W. Zhou, H. Chen, Z. Zhou, Y. Wang, B. Su, H. You, T. Zhang, X. Li, H. Song, C. Li, T. Sun and C. Jiang, *Adv. Sci.*, 2021, **8**, 2101526.
10 K. Pekayvaz, C. Gold, P. Hoseinpour, A. Engel, A. Martinez-Navarro, L. Eivers, R. Coletti, M. Joppich, F. Dionísio, R. Kaiser, L. Tomas, A. Janjic, M. Knott, F. Mehari, V. Polewka, M. Kirschner, A. Boda, L. Nicolai, H. Schulz, A. Titova, B. Kilani, M. Lorenz, G. Fingerle-Rowson, R. Bucala, W. Enard, R. Zimmer, C. Weber, P. Libby, C. Schulz, S. Massberg and K. Stark, *Immunity*, 2023, **56**, 2325–2341.
11 F. Bonacina, X. Zhang, N. Manel, L. Yvan-Charvet, B. Razani and G. D. Norata, *Nat. Rev. Cardiol.*, 2025, **22**, 149–164.
12 Z. Wang, X. Li, A. K. Moura, J. Z. Hu, Y.-T. Wang and Y. Zhang, *Cells*, 2025, **14**, 183.
13 I. Sergin, S. Bhattacharya, X. Zhang, T. D. Evans, B. Dehestani, R. Emanuel and B. Razani, *Arterioscler., Thromb., Vasc. Biol.*, 2016, **36**, 1.
14 A. Skeyni, A. Pradignac, R. L. Matz, J. Terrand and P. Boucher, *J. Appl. Physiol.*, 2023, **326**, C473–C486.
15 J. An, L. Ouyang, C. Yu, S. M. Carr, T. Ramprasath, Z. Liu, P. Song, M.-H. Zou and Y. Ding, *Theranostics*, 2023, **13**, 2825–2842.
16 P. Kumar, E. Laurence, D. K. Crossman, D. G. Assimos, M. P. Murphy and T. Mitchell, *Redox Biol.*, 2023, **67**, 102919.
17 C. W. Chae, Y. J. Hyeon, L. J. Ryong, P. J. Yong, C. J. Hyeon, J. Y. Hyun, C. G. Euhn, L. H. Jik and H. J. and Han, *Autophagy*, 2023, **19**, 2752–2768.
18 W. Li, S. Yin, Y. Shen, H. Li, L. Yuan and X.-B. Zhang, *J. Am. Chem. Soc.*, 2023, **145**, 3736–3747.
19 L. Weng, W.-S. Tang, X. Wang, Y. Gong, C. Liu, N.-N. Hong, Y. Tao, K.-Z. Li, S.-N. Liu, W. Jiang, Y. Li, K. Yao, L. Chen, H. Huang, Y.-Z. Zhao, Z.-P. Hu, Y. Lu, H. Ye, X. Du, H. Zhou, P. Li and T.-J. Zhao, *Nat. Commun.*, 2024, **15**, 133.
20 Q. Zhang, X. Shen, X. Yuan, J. Huang, Y. Zhu, T. Zhu, T. Zhang, H. Wu, Q. Wu, Y. Fan, J. Ni, L. Meng, A. He, C. Shi, H. Li, Q. Hu, J. Wang, C. Chang, F. Huang, F. Li, M. Chen, A. Liu, S. Ye, M. Zheng and H. Fang, *Nat. Commun.*, 2024, **15**, 3213.
21 Y. Yang, J. Yang, J. Zhu, X. Chen, L. Zhou, W. Ma and Y. Lin, *Bioact. Mater.*, 2024, **39**, 191–205.
22 A. Debroy, A. K. Sinha, C. Maity, M. Pulimi, W. J. G. M. Peijnenburg and A. Mukherjee, *J. Hazard. Mater.*, 2025, **486**, 137034.
23 A. S. Ondracek, T. Afonyushkin, A. Aszlan, S. Taqi, T. Koller, T. Artner, F. Porsch, U. Resch, S. Sharma, T. Scherz, A. Spittler, M. Haertinger, T. M. Hofbauer, M. Ozsvar-Kozma, V. Seidl, D. Beitzke, M. Krueger, C. Testori, I. M Lang and C. J. Binder, *Eur. Heart J.*, 2025, **46**, 926–939.
24 X. Liu, Z. Li, Z. Wang, K. Wang, X. Rong, Y. Wang, T. Yan, W. Shu, C. Liu and B. Zhu, *Bioorganomet. Chem.*, 2025, **162**, 108585.

25 F. Bonacina, X. Zhang, N. Manel, L. Yvan-Charvet, B. Razani and G. D. Norata, *Nat. Rev. Cardiol.*, 2025, **22**, 149–164.
26 H. Tao, J. Huang, P. G. Yancey, V. Yermalitsky, J. L. Blakemore, Y. Zhang, L. Ding, I. Zagol-Ikapitte, F. Ye, V. Amarnath, O. Boutaud, J. A. Oates, L. J. Roberts, S. S. Davies and M. F. Linton, *Nat. Commun.*, 2020, **11**, 4084.
27 J. Li, H. Yu, J. Zhao, X. Qiao, X. Chen, Z. Lu, Q. Li, H. Lin, W. Wu, W. Zeng, Z. Yang and Y. Feng, *Nano Lett.*, 2024, **24**, 7792–7799.
28 W. Wang, S. Han, J. Ren, X. Xiao, J. Chen, R. You, G. Zhang and Y. Lu, *Cellulose*, 2024, **31**, 3717–3728.
29 Y. He, H. Wang, C. He, R. Zeng, F. Cheng, Y. Hao, S. Chen and P. Zhang, *Sens. Actuators, B*, 2025, **425**, 136983.
30 X. Wu, H. Cai, R. Liao, A. C Tedesco, Z. Li, F. Wang and H. Bi, *Small*, 2024, **20**, 2400671.
31 Y. Tian, Z. Zhou, J. Gong, J. Li, C. He, J. Chen, S. Chen, R. Zeng, Z. Mao and P. Zhang, *Sens. Actuators, B*, 2023, **394**, 134421.
32 R. Zou, Y. Yu, H. Pan, P. Zhang, F. Cheng, C. Zhang, S. Chen, J. Chen and R. Zeng, *ACS Appl. Mater. Interfaces*, 2022, **14**, 16746–16754.
33 D. Su, R. Zhang, X. Wang, Q. Ding, F. Che, Z. Liu, J. Xu, Y. Zhao, K. Ji, W. Wu, C. Yan, P. Li and B. Tang, *J. Am. Chem. Soc.*, 2023, **145**, 22609–22619.
34 H. Liu, P. Zhang, C. Zhang, J. Chen and J.-H. Jiang, *ACS Appl. Mater. Interfaces*, 2020, **12**, 45822–45829.
35 P. Zhang, X. Nie, M. Gao, F. Zeng, A. Qin, S. Wu and B. Z. Tang, *Mater. Chem. Front.*, 2017, **1**, 838–845.